Observation of sequential Υ suppression in Au+Au collisions at $\sqrt{s_{\mathrm{NN}}} = 200$ GeV with the STAR experiment

(The STAR Collaboration)

We report on measurements of sequential Υ suppression in Au+Au collisions at $\sqrt{s_{\mathrm{NN}}} = 200$ GeV with the STAR detector at the Relativistic Heavy Ion Collider (RHIC) through both the di-electron and di-muon channels. In the 0-60% centrality class, the nuclear modification factors (R_{AA}), which quantify the level of yield suppression in heavy-ion collisions compared to $p+p$ collisions, for $\Upsilon(1S)$ and $\Upsilon(2S)$ are 0.40 ± 0.03 (stat.) ± 0.03 (sys.) ± 0.07 (norm.) and 0.26 ± 0.07 (stat.) ± 0.02 (sys.) ± 0.04 (norm.), respectively, while the upper limit of the $\Upsilon(3S)$ R_{AA} is 0.20 at a 95% confidence level. This observation provides experimental evidence that the $\Upsilon(3S)$ is significantly more suppressed than the $\Upsilon(1S)$ at RHIC. The level of suppression for $\Upsilon(1S)$ is comparable to that observed at the much higher collision energy at the Large Hadron Collider. These results point to the creation of a deconfined medium at RHIC whose temperature is sufficiently high to strongly suppress excited Υ states.

Keywords: STAR, heavy-ion collisions, Υ suppression

arXiv:2207.06568v1 [nucl-ex] 14 Jul 2022

A primary goal of the Relativistic Heavy Ion Collider (RHIC) is to create and study the properties of the Quark-Gluon Plasma (QGP), whose relevant degrees of freedom are deconfined partons, not hadrons [1–4], in high-energy heavy-ion collisions. Quantum chromodynamics (QCD) predicts that, in such a deconfined state, the confining potential of a heavy quark-antiquark pair is color-screened by surrounding partons [5], leading to dissociation of quarkonium states. Such a static dissociation is expected to happen when the quarkonium size is larger than the Debye screening length of the medium [6], which is inversely proportional to the medium temperature. In addition, dynamic dissociation, arising from inelastic scatterings between quarkonia and medium constituents, can also lead to quarkoninum breakup, whose impact becomes more profound with increasing medium temperature and for quarkonia of smaller binding energies [7–9]. Consequently, different quarkonium states suffer from different levels of suppression in the QGP ("sequential suppression") depending on their sizes and the medium temperature [8, 10, 11]. Heavy quarkonia are therefore considered promising probes to study the color deconfinement, in-medium heavy quark potential, and the QGP's thermodynamic properties.

Strong suppression of J/ψ mesons at high transverse momenta (p_{T}) due to dissociation has been observed at both RHIC and the Large Hadron Collider (LHC) [12–15]. The excited charmonium state ($\psi(2S)$), which has a smaller binding energy than the J/ψ, is further suppressed [16, 17], consistent with the sequential suppression picture. Compared to charmonia, bottomonia ($\Upsilon(1S)$, $\Upsilon(2S)$, and $\Upsilon(3S)$), with $\Upsilon(1S)$ being the most strongly bound and $\Upsilon(3S)$ the least, provide a larger dynamic range in probing the QGP. According to lattice QCD calculations based on the complex quark-antiquark potential, the span of the dissociation temperature for the three bottomonium states is about a factor of four larger than that for the two charmoinum states [8]. Furthermore, bottomonia are considered cleaner probes than charmonia despite their smaller production rates. Due

to the smaller production cross section of $b\bar{b}$ compared to that of $c\bar{c}$, the regeneration, *i.e.* deconfined heavy quark-antiquark pairs combining into bound quarkonium states, contributes less than 10% to $\Upsilon(1S)$ [18], and about 50% to J/ψ [19] in head-on Au+Au collisions at the center-of-mass energy ($\sqrt{s_{\mathrm{NN}}}$) of 200 GeV. The relative contribution of regeneration increases to about 25% for $\Upsilon(2S+3S)$, denoting combined $\Upsilon(2S)$ and $\Upsilon(3S)$ states [18]. In addition, the $\Upsilon(1S)$ absorption cross sections by π and ρ mesons are roughly a factor of 5 to 10 smaller than those of J/ψ[20, 21], rendering hadronic breakup unimportant for $\Upsilon(1S)$. When interpreting Υ suppression measured in heavy-ion collisions, Cold Nuclear Matter (CNM) effects, arising from the presence of nuclei in the collision but not related to the QGP, need to be taken into account [22–24]. Measurements in d+Au collisions at RHIC [25] show a hint of suppression for three Υ states combined, while more differential measurements in p+Pb collisions at the LHC [26–29] find an increasing suppression towards low p_{T}, and that excited Υ states are more suppressed than the ground state.

The sequential suppression of the three Υ states have been observed at the LHC [30–32]. In Pb+Pb collisions at $\sqrt{s_{\mathrm{NN}}} = 5.02$ TeV [31], $\Upsilon(2S)$ is further suppressed by about a factor of 3.2 than $\Upsilon(1S)$, while an additional suppression factor of approximately 5.3 is found for $\Upsilon(3S)$ compared to $\Upsilon(2S)$. In Au+Au collisions at $\sqrt{s_{\mathrm{NN}}} = 200$ GeV [25] and U+U collisions at $\sqrt{s_{\mathrm{NN}}} = 193$ GeV [33] at RHIC, previous STAR measurements revealed a hint of stronger suppression for $\Upsilon(2S+3S)$ compared to $\Upsilon(1S)$, with a significance of less than 1.5σ for the $\Upsilon(2S+3S)$ measurement. To fully utilize the constraining power of quarkoinum sequential suppression on medium's properties at RHIC, differential measurements of ground and excited Υ states separately with improved precision are crucially needed. Such measurements are also complementary to similar results at the LHC to provide stringent tests to theoretical calculations, given that media of different temperatures are created at the two facilities.

In this letter, we report on the latest measurements of

the suppression for $\Upsilon(1S)$, $\Upsilon(2S)$ and $\Upsilon(3S)$ through both di-electron and di-muon decay channels in Au+Au collisions at $\sqrt{s_{NN}} = 200$ GeV, corresponding to integrated luminosities of 2.3 nb^{-1} and 27 nb^{-1}, respectively. The suppression is quantified with the nuclear modification factor (R_{AA}), which is the ratio of the quarkonium yield measured in nucleus-nucleus (A+A) collisions to that in $p+p$ collisions, scaled by the average number of binary nucleon-nucleon collisions (N_{coll}). Results are presented as a function of the collision centrality or the Υ p_T, where central (peripheral) collisions correspond to incoming nuclei most (least) overlapping with each other. They are compared to those measured in Pb+Pb collisions at $\sqrt{s_{NN}}$ = 5.02 TeV [31], as well as model calculations [18, 34–36].

The subsystems of the STAR experiment [37] most relevant for this analysis are the Time Projection Chamber (TPC) [38], the Barrel Electromagnetic Calorimeter (BEMC) [39] and the Muon Telescope Detector (MTD) [13, 40]. The TPC is used for track reconstruction and particle identification (PID), while the BEMC and MTD are used for triggering on and identifying electrons and muons, respectively. The TPC and the BEMC have a full azimuthal coverage within the pseudorapidity range of $|\eta| < 1$. The MTD, fully installed since 2014, covers about 45% in azimuth within $|\eta| < 0.5$. For the $\Upsilon \rightarrow e^+e^-$ analysis, Au+Au collision data were taken with the BEMC trigger, requiring the transverse energy deposition in a single tower above 3.5 GeV, in 2011 RHIC run. Electrons with $p_T > 3.5$ GeV/c are selected based on their ionization energy loss (dE/dx) measured in the TPC. A cut on the ratio of energy deposition in BEMC over momentum (E/p) is also applied to further reject hadrons. In addition, one of the daughter electrons from the Υ decay must fire the BEMC trigger. For the $\Upsilon \rightarrow \mu^+\mu^-$ analysis, Au+Au data were taken with the MTD di-muon trigger in 2014 and 2016 RHIC runs. The di-muon trigger requires presence of two muon candidates, identified based on the particles' flight time, in the MTD. Both muons from Υ decays are required to fire the online trigger. In the offline analysis, the leading muon is required to have p_T above 4 GeV/c and the sub-leading above 1.5 GeV/c. Besides dE/dx from the TPC, muon candidates are identified utilizing position and timing information measured by the MTD [13, 41].

A Glauber model simulation [42] is used for centrality classification since, unlike data, it is unaffected by trigger inefficiency for peripheral events. The simulated distribution is matched to the charged-particle multiplicity within $|\eta| < 0.5$ measured in the TPC at large multiplicity values. The centrality classes are then determined by dividing the matched multiplicity distribution from the Glauber simulation into percentiles of the total inelastic cross section. The average number of participating nucleons (N_{part}) and N_{coll} are calculated for each centrality class. Data are divided into three centrality bins: 0-10%, 10-30%, and 30-60%, as well as three p_T bins: 0-2 GeV/c, 2-5 GeV/c, and 5-10 GeV/c.

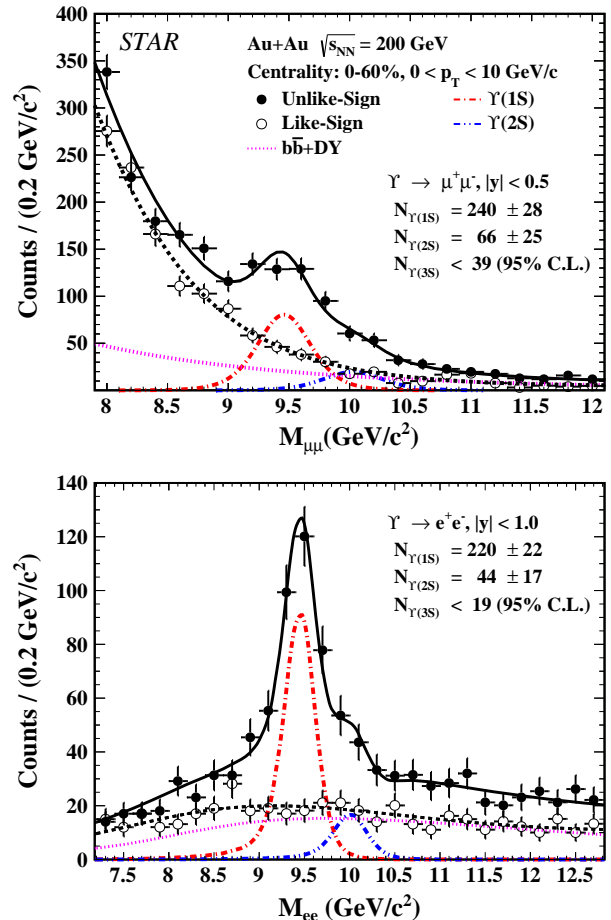The invariant mass spectra of the Υ candidates are

FIG. 1. Invariant mass distributions of Υ candidates for $0 < p_T < 10$ GeV/c reconstructed via the di-muon channel within $|y| < 0.5$ (top) and the di-electron channel within $|y| < 1$ (bottom). Unlike-sign and like-sign distributions are shown as full and open circles, respectively. Solid lines are fits to the unlike-sign distributions, while lines of other styles represent individual components included in the fit (more details in the text).

reconstructed from the $\Upsilon \rightarrow \mu^+\mu^-$ channel within the rapidity range of $|y| < 0.5$ and from the $\Upsilon \rightarrow e^+e^-$ channel within $|y| < 1$. Figure 1 shows the unlike-sign lepton-pair distributions (full circles), along with like-sign ones (open circles) which are used for determining the shape, modeled with an exponential function, and amplitude of the combinatorial background. A simultaneous unbinned maximum-likelihood fit is performed on both the unlike-sign and like-sign distributions to obtain the yields for the three Υ states. The lineshapes of the mass peaks for Υ(nS) are determined from GEANT3 simulations [43] of the STAR detector, in which the $\Upsilon \rightarrow \mu^+\mu^-$ or $\Upsilon \rightarrow e^+e^-$ decays are embedded into Au+Au collision events, and reconstructed in the same way as real data. The track momentum resolution in the simulation is further tuned to match the J/ψ width as a func-

tion of p_T reconstructed in real data. The widths of the main peaks for $\Upsilon(1S)$ are 221 MeV/c^2 and 129 MeV/c^2 for the di-muon and di-electron channels, respectively. The shape of the correlated background from $b\bar{b}$ decays and Drell-Yan processes is determined with PYTHIA6 simulations [44] incorporating realistic detector response while its yield is left as a free fit parameter. The different background shapes between the two decay channels are mainly driven by the different kinematic cuts applied to the lepton candidates. With current statistics, no $\Upsilon(3S)$ signal is observed in either decay channel, and therefore only the upper limits of $\Upsilon(3S)$ yields are estimated by the Feldman-Cousins method [45] at a 95% confidence level.

The detector acceptance and the TPC tracking efficiency are determined based on aforementioned embedding simulations. In the $\Upsilon \to e^+e^-$ analysis, efficiencies related to the BEMC trigger, and to the electron identification through the dE/dx and E/p cuts, are evaluated using a pure electron sample from gamma conversions in the data. Similarly in the $\Upsilon \to \mu^+\mu^-$ analysis, a pure muon sample from J/ψ decays is used to evaluate the efficiencies for muon PID based on dE/dx and the timing information recorded in the MTD. The embedding technique is used to estimate the additional PID efficiency related to using the position information of muon tracks on the MTD surface, as well as the geometrical acceptance of the MTD. The MTD response efficiency is obtained from cosmic-ray data, while the MTD trigger efficiency is calculated using the $p+p$ collision data taken in 2015 in which the trigger system is similar to that used in this analysis. The latter is justified by the fact that the MTD occupancy is very low even in 0-10% central Au+Au collisions [13] (rendering the multiplicity difference between $p+p$ and Au+Au collisions irrelevant) and that the MTD trigger efficiency is close to 100% in 2015 $p+p$ data due to the very loose online trigger requirement [46]. In the $\Upsilon \to \mu^+\mu^-$ analysis, although the signal extraction is performed on combined data sets taken in 2014 and 2016, the Υ reconstruction efficiency is calculated individually and combined using the sampled luminosities in each year as weights.

Several sources of systematic uncertainty are considered. Different variations are made in the signal extraction procedure and the maximum deviations are taken as the systematic uncertainties. The fit range is varied, as well as the functional form used to model the combinatorial background. The uncertainty in the track momentum resolution, determined from reproducing the J/ψ signal width in data, is also taken into account. Furthermore, the shape of the residual background is varied by using only Drell-Yan or $b\bar{b}$ processes, and by decorrelating the lepton pairs from $b\bar{b}$ decays in momentum space, mimicking possible hot-medium effects. For the di-electron (di-muon) analysis, the resulting uncertainty varies between 2.9-9.2% (2.8-9.6%) and 3.9-25.6% (2.6-200%) for $\Upsilon(1S)$ and $\Upsilon(2S)$ in different centrality and p_T bins, and is 6.2 (12.0) in absolute value for $\Upsilon(3S)$ yield integrated

over p_T in 0-60% centrality. Another major source of uncertainty arises from the tracking and PID efficiencies. This is evaluated by varying the track quality and PID cuts simultaneously in data analysis and simulation, correcting the raw yields, and taking the root mean square of the corrected yield distribution as the uncertainty. For efficiencies evaluated using data-driven methods, statistical errors of the data samples are treated as systematic uncertainties. The overall efficiency uncertainties apply equally to all three Υ states, and they vary from 3.1% to 15.3% (3.4% to 13.2%) depending on centrality and p_T for the di-electron (di-muon) analysis. Finally, the individual sources are added in quadrature to obtain the total systematic uncertainties.

The reference $\Upsilon(1S+2S+3S)$ production cross section in $p+p$ collisions at $\sqrt{s} = 200$ GeV is $\frac{d\sigma}{dy}|_{|y|<0.5} = 75 \pm 15$ pb, obtained by combining STAR and PHENIX measurements [25, 47, 48]. The error includes both statistical and systematic uncertainties. The cross sections of individual Υ states are calculated based on the total cross section and their yield ratios from world data [49]. To obtain the reference cross sections in different p_T bins, the measured Υ p_T spectra at lower and higher collision energies [30, 50–52] than 200 GeV are parameterized with the functional form $C \times p_T/(e^{p_T/T}+1)$ [33], where C is a normalization factor and T is the shape parameter. The dependence of T on $\log(\sqrt{s})$ is fit with both a linear and a power-law function, and the average interpolated T values at $\sqrt{s} = 200$ GeV from the two fits, i.e., 1.40 ± 0.06 GeV/c and 1.51 ± 0.10 GeV/c for $\Upsilon(1S)$ and $\Upsilon(2S)$, are obtained. Systematic uncertainties arise from the uncertainties on the measured Υ spectra and the functional form used for interpolation.

The R_{AA} of individual Υ states in Au+Au collisions at $\sqrt{s_{NN}} = 200$ GeV is obtained by combining results from di-muon and di-electron channels using the inverse of statistical errors squared as weights, since the results from the two analyses are consistent despite the different rapidity coverages. Similarly, no strong dependence of Υ R_{AA} on rapidity within $|y| < 1$ is observed at the LHC [31]. The systematic uncertainties are combined assuming they are uncorrelated between the two channels.

Figure 2 shows the R_{AA} of $\Upsilon(1S)$ and $\Upsilon(2S)$ as a function of N_{part} in three centrality intervals. The $\Upsilon(3S)$ R_{AA} is consistent with zero, and therefore the upper limit with a 95% confidence level is estimated to be 0.20 and shown in Fig. 2 for the 0-60% centrality. All of the Υ states are suppressed in all three centrality intervals with a hint of increasing suppression from the 30-60% to the 0-10% centrality bin, consistent with the expected increasing hot medium effect. In the 0-60% centrality class, $\Upsilon(3S)$ is significantly more suppressed than $\Upsilon(1S)$, given that even the upper limit of $\Upsilon(3S)$ R_{AA} at a 99% confidence level, i.e. 0.29, is still lower than the $\Upsilon(1S)$ R_{AA} of 0.40 ± 0.03 (stat.) ± 0.03 (sys.) ± 0.07 (norm.). Here, the normalization uncertainty includes uncertainties in $p+p$ reference and N_{coll}. A hint is seen that the level of suppression for $\Upsilon(2S)$, whose R_{AA} is 0.26 ± 0.07 (stat.) $\pm$
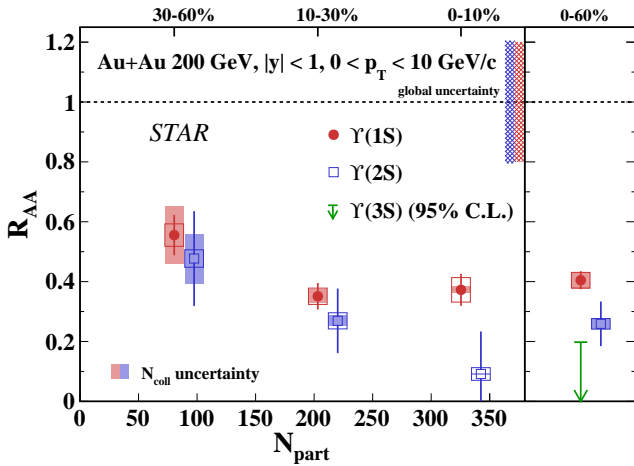
FIG. 2. Left: Υ(1S) (circles) and Υ(2S) (squares) $R_{\rm AA}$ as a function of $N_{\rm part}$ for $p_{\rm T} < 10$ GeV/c. The vertical bars on data points indicate statistical errors, while the systematic uncertainties are shown as boxes. Shadowed bands around each marker depict the systematic uncertainties from $N_{\rm coll}$. The bands at unity show the relative uncertainties of the reference $p+p$ yields. Right: $R_{\rm AA}$ for various Υ states, including the 95% upper limit for Υ(3S), in 0-60% Au+Au collisions.

0.02 (sys.) $\pm$ 0.04 (norm.), is between Υ(1S) and Υ(3S). These results are consistent with a sequential suppression pattern at RHIC, similar to that observed at the LHC [31].

The Au+Au results are compared to similar measurements in Pb+Pb collisions at $\sqrt{s_{\rm NN}} = 5.02$ TeV [31] in Fig. 3. Υ(1S) exhibits a similar magnitude of suppression at the two collision energies that differ by about a factor of 25, while there is a hint that the Υ(2S) might be less suppressed at RHIC in peripheral collisions. It is plausible that the suppression of inclusive Υ(1S) arises mainly from the suppression of excited states that feed down to Υ(1S) [53] as well as CNM effects [25, 27, 29], while the primordial Υ(1S) remains largely unaffected by the QGP in both 200 GeV Au+Au and 5.02 TeV Pb+Pb collisions. Figure 3 also shows the comparison between data and two calculations based on Open Quantum System (OQS) plus potential Non-Relativistic QCD (pNRQCD) [54–56] and a transport model [18]. The OQS+pNRQCD model solves a Lindblad equation for the evolution of the quarkonium reduced density matrix using the pN-RQCD effective field theory [56]. The temperatures of the medium at time of 0.25 fm/c in central collisions are 455 MeV and 630 MeV for 200 GeV Au+Au and 5.02 TeV Pb+Pb collisions, respectively. Correlated regeneration and feed-down contributions from excited states are included, but the CNM effects are not. Systematic uncertainties stem from variations in the transport coefficients suggested by lattice data. On the other hand, the transport model employs a temperature-dependent binding energy based on microscopic T-matrix calculations, and uses a kinetic rate equation to simulate the time evo-
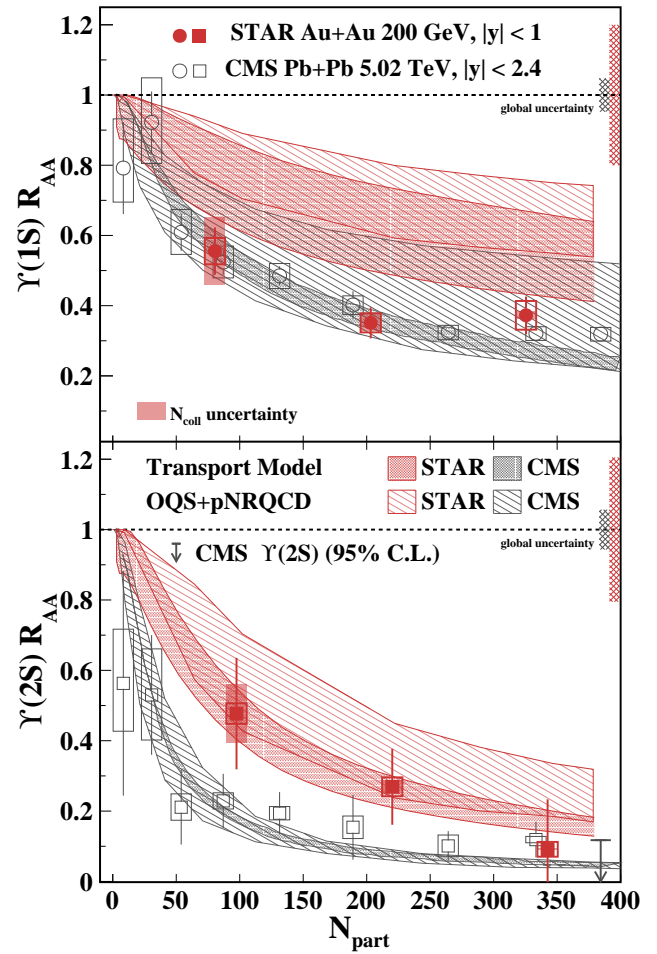

FIG. 3. Υ(1S) (top) and Υ(2S) (bottom) $R_{\rm AA}$ as a function of $N_{\rm part}$ for $p_{\rm T} < 10$ GeV/c, compared to similar measurements in Pb+Pb collisions at $\sqrt{s_{\rm NN}} = 5.02$ TeV (open symbols), as well as model calculations (bands). The two bands at unity indicate the global uncertainties with the left one for CMS and the right one for STAR.

lution of bottomonium abundances including dissociation and regeneration contributions. The initial temperatures reached in central collisions are 310 MeV and 594 MeV for Au+Au and Pb+Pb collisions. Both feed-down and CNM effects are taken into account, and the model uncertainties arise from the range of CNM effects guided by data [25]. For the Υ(1S) $R_{\rm AA}$, both models are systematically above the STAR measurement with the transport model closer to data, while providing a good description for the CMS measurement. For Υ(2S), model calculations are consistent with the STAR measurement within uncertainties, but tend to undershoot CMS measurement towards central collisions.

Figure 4 shows the $R_{\rm AA}$ for Υ(1S) and Υ(2S) as a function of $p_{\rm T}$. No significant dependence on $p_{\rm T}$ is observed. One model uses a set of coupled Boltzmann equations to simultaneously describe the in-medium evolution of heavy quarks and quarkonia in the QGP [36]. It incorporates elastic and inelastic scatterings of heavy quarks
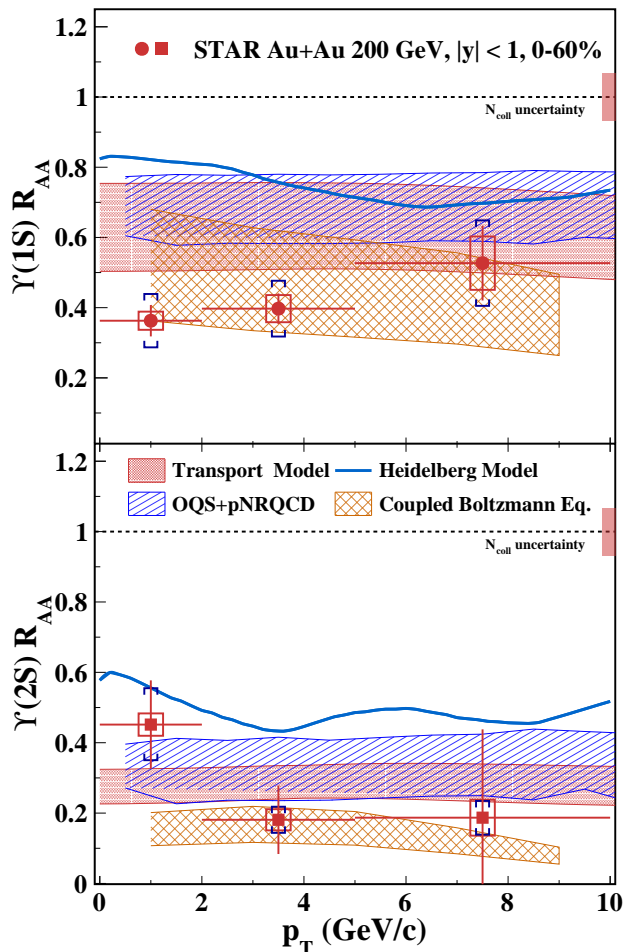
FIG. 4. $\Upsilon(1S)$ (top) and $\Upsilon(2S)$ (bottom) R_{AA} as a function of p_T in the 0-60% centrality, compared to different model calculations. The boxes and brackets around the data points represent systematic uncertainties from Au+Au analysis and $p+p$ reference, respectively. The band at unity shows the uncertainty in N_{coll}.

with medium constituents, as well as quarkonium dissociation and regeneration. The dominant uncertainty arises from the nuclear parton distribution function used for estimating CNM effects. The model calculations are consistent with data within uncertainties. The Heidelberg model [35], which accounts for the dissociation effect as well as feed-down from higher states, overshoots data, partly due to the lack of CNM effects.

In summary, we report on the measurements of Υ production in Au+Au collisions at $\sqrt{s_{NN}} = 200$ GeV via both the di-electron and di-muon channels with the STAR experiment. The R_{AA} for $\Upsilon(1S)$ and $\Upsilon(2S)$ is measured as functions of collision centrality and p_T, while the upper limit on the $\Upsilon(3S)$ R_{AA} is derived with the collision centrality and p_T integrated. In the 0-60% centrality bin, a sequential suppression pattern is observed given that the $\Upsilon(3S)$ is significantly more suppressed than the $\Upsilon(1S)$, and that the $\Upsilon(2S)$ R_{AA} is between those of the $\Upsilon(1S)$ and $\Upsilon(3S)$. No clear p_T dependence of the suppression is observed for $\Upsilon(1S)$ and $\Upsilon(2S)$. The magnitude of the suppression for $\Upsilon(1S)$ in Au+Au collisions at $\sqrt{s_{NN}} = 200$ GeV is comparable to that measured in Pb+Pb collisions at $\sqrt{s_{NN}} = 5.02$ TeV, which is different from model calculations. A hint of less $\Upsilon(2S)$ suppression at RHIC than at the LHC is observed for peripheral collisions. Results presented in this paper can help further constrain model calculations on bottomonium suppression in heavy-ion collisions and improve our understanding of the thermal and dynamical properties of the QGP at RHIC.

[1] J. Adams, et al. (STAR), Experimental and theoretical challenges in the search for the quark gluon plasma: The STAR Collaboration's critical assessment of the evidence from RHIC collisions, Nucl. Phys. A 757 (2005) 102–83.

[2] K. Adcox, et al. (PHENIX), Formation of dense partonic matter in relativistic nucleus-nucleus collisions at RHIC: Experimental evaluation by the PHENIX collaboration, Nucl. Phys. A 757 (2005) 184–283.

[3] B. Back, et al. (PHOBOS), The PHOBOS perspective on discoveries at RHIC, Nucl. Phys. A 757 (2005) 28–101.

[4] I. Arsene, et al. (BRAHMS), Quark gluon plasma and color glass condensate at RHIC? The Perspective from the BRAHMS experiment, Nucl. Phys. A 757 (2005) 1–27.

[5] T. Matsui, H. Satz, J/ψ Suppression by Quark-Gluon Plasma Formation, Phys. Lett. B178 (1986) 416.

[6] H. Satz, Color Screening in SU(N) Gauge Theory at Finite Temperature, Nucl. Phys. A 418 (1984) 447C–65.

[7] M. Laine, O. Philipsen, P. Romatschke, M. Tassler, Real-time static potential in hot QCD, JHEP 03 (2007) 054.

[8] Y. Burnier, O. Kaczmarek, A. Rothkopf, Quarkonium at finite temperature: Towards realistic phenomenology from first principles, JHEP 12 (2015) 101.

[9] S. Chen, M. He, Gluo-dissociation of heavy quarkonium in the quark-gluon plasma reexamined, Phys. Rev. C 96 (2017) 034901.

[10] S. Digal, P. Petreczky, H. Satz, Quarkonium feed down and sequential suppression, Phys. Rev. D 64 (2001) 094015.

[11] A. Mocsy, P. Petreczky, Color screening melts quarkonium, Phys. Rev. Lett. 99 (2007) 211602.

[12] A. Adare, et al. (PHENIX), J/ψ Production vs Centrality, Transverse Momentum, and Rapidity in Au+Au Collisions at $\sqrt{s_{NN}}$ = 200 GeV, Phys. Rev. Lett. 98 (2007) 232301.

[13] J. Adam, et al. (STAR), Measurement of inclusive J/ψ suppression in Au+Au collisions at $\sqrt{s_{NN}}$ = 200 GeV through the dimuon channel at STAR, Phys. Lett. B 797 (2019) 134917.

[14] J. Adam, et al. (ALICE), Inclusive, prompt and non-prompt J/ψ production at mid-rapidity in Pb-Pb collisions at $\sqrt{s_{NN}}$ = 2.76 TeV, JHEP 07 (2015) 051.

[15] S. Acharya, et al. (ALICE), Centrality and transverse momentum dependence of inclusive J/ψ production at midrapidity in Pb–Pb collisions at $\sqrt{s_{NN}}$ = 5.02 TeV, Phys. Lett. B 805 (2020) 135434.

[16] A. M. Sirunyan, et al. (CMS), Relative Modification of Prompt ψ(2S) and J/ψ Yields from pp to PbPb Collisions at $\sqrt{s_{NN}}$ = 5.02 TeV, Phys. Rev. Lett. 118 (2017) 162301.

[17] M. Aaboud, et al. (ATLAS), Prompt and non-prompt J/ψ and ψ(2S) suppression at high transverse momentum in 5.02 TeV Pb+Pb collisions with the ATLAS experiment, Eur. Phys. J. C 78 (2018) 762.

[18] X. Du, R. Rapp, M. He, Color screening and regeneration of bottomonia in high-energy heavy-ion collisions, Phys. Rev. C 96 (2017) 054901.

[19] X. Zhao, R. Rapp, Charmonium in Medium: From Correlators to Experiment, Phys. Rev. C 82 (2010) 064905.

[20] Z.-W. Lin, C. M. Ko, A Model for J/ψ absorption in hadronic matter, Phys. Rev. C 62 (2000) 034903.

[21] Z.-W. Lin, C. M. Ko, Upsilon absorption in hadronic matter, Phys. Lett. B 503 (2001) 104–12.

[22] E. G. Ferreiro, F. Fleuret, J. P. Lansberg, A. Rakotozafindrabe, Centrality, rapidity and transverse-Momentum dependence of cold nuclear matter effects on J/ψ production in dAu, CuCu and AuAu collisions at $\sqrt{s_{NN}}$ = 200 GeV, Phys. Rev. C 81 (2010) 064911.

[23] F. Arleo, S. Peigné, Quarkonium suppression in heavy-ion collisions from coherent energy loss in cold nuclear matter, JHEP 10 (2014) 073.

[24] S. Gavin, R. Vogt, Charmonium suppression by Co-mover scattering in Pb+Pb collisions, Phys. Rev. Lett. 78 (1997) 1006–9.

[25] L. Adamczyk, et al. (STAR), Suppression of Υ production in d+Au and Au+Au collisions at $\sqrt{s_{NN}}$ = 200 GeV, Phys. Lett. B 735 (2014) 127–37. [Erratum: Phys.Lett.B 743, 537–541 (2015)].

[26] S. Acharya, et al. (ALICE), Υ production in p–Pb collisions at $\sqrt{s_{NN}}$ = 8.16 TeV, Phys. Lett. B 806 (2020) 135486.

[27] M. Aaboud, et al. (ATLAS), Measurement of quarkonium production in proton–lead and proton–proton collisions at 5.02 TeV with the ATLAS detector, Eur. Phys. J. C 78 (2018) 171.

[28] R. Aaij, et al. (LHCb), Study of Υ production in pPb collisions at $\sqrt{s_{NN}}$ = 8.16 TeV, JHEP 11 (2018) 194. [Erratum: JHEP 02, 093 (2020)].

[29] A. Tumasyan, et al. (CMS), Nuclear modification of Υ states in pPb collisions at $\sqrt{s_{NN}}$ = 5.02 TeV (2022).

[30] V. Khachatryan, et al. (CMS), Suppression of Υ(1S), Υ(2S) and Υ(3S) production in PbPb collisions at $\sqrt{s_{NN}}$ = 2.76 TeV, Phys. Lett. B 770 (2017) 357–79.

[31] A. M. Sirunyan, et al. (CMS), Measurement of nuclear modification factors of Υ(1S), Υ(2S), and Υ(3S) mesons in PbPb collisions at $\sqrt{s_{NN}}$ = 5.02 TeV, Phys. Lett. B 790 (2019) 270–93.

[32] S. Acharya, et al. (ALICE), Υ production and nuclear modification at forward rapidity in Pb-Pb collisions at $\sqrt{s_{NN}}$ = 5.02 TeV, Phys. Lett. B 822 (2021) 136579.

[33] L. Adamczyk, et al. (STAR), Υ production in U+U collisions at $\sqrt{s_{NN}}$ = 193 GeV measured with the STAR experiment, Phys. Rev. C 94 (2016) 064904.

[34] B. Krouppa, A. Rothkopf, M. Strickland, Bottomonium suppression using a lattice QCD vetted potential, Phys. Rev. D 97 (2018) 016017.

[35] J. Hoelck, F. Nendzig, G. Wolschin, In-medium Υ suppression and feed-down in UU and PbPb collisions, Phys. Rev. C 95 (2017) 024905.

[36] X. Yao, W. Ke, Y. Xu, S. A. Bass, B. Müller, Coupled Boltzmann Transport Equations of Heavy Quarks and Quarkonia in Quark-Gluon Plasma, JHEP 01 (2021) 046.

[37] K. Ackermann, et al. (STAR), STAR detector overview, Nucl. Instrum. Meth. A 499 (2003) 624–32.

[38] M. Anderson, et al., The Star time projection chamber: A Unique tool for studying high multiplicity events at RHIC, Nucl. Instrum. Meth. A 499 (2003) 659–78.

[39] M. Beddo, et al. (STAR), The STAR barrel electromagnetic calorimeter, Nucl. Instrum. Meth. A 499 (2003) 725–39.

[40] L. Ruan, et al., Perspectives of a Midrapidity Dimuon Program at RHIC: A Novel and Compact Muon Telescope Detector, J. Phys. G 36 (2009) 095001.

[41] T. C. Huang, et al., Muon Identification with Muon Telescope Detector at the STAR Experiment, Nucl. Instrum. Meth. A 833 (2016) 88–93.

[42] M. L. Miller, K. Reygers, S. J. Sanders, P. Steinberg, Glauber modeling in high energy nuclear collisions, Ann. Rev. Nucl. Part. Sci. 57 (2007) 205–43.

[43] R. Brun, F. Bruyant, M. Maire, A. C. McPherson, P. Zanarini, GEANT3, CERN-DD-EE-84-1 (1987).

[44] T. Sjostrand, S. Mrenna, P. Z. Skands, PYTHIA 6.4 Physics and Manual, JHEP 05 (2006) 026.

[45] G. J. Feldman, R. D. Cousins, Unified approach to the classical statistical analysis of small signals, Phys. Rev. D 57 (1998) 3873–89.

[46] M. Abdallah, et al. (STAR), Measurement of cold nuclear matter effects for inclusive J/ψ in p+Au collisions at $\sqrt{s_{NN}}$ = 200 GeV, Phys. Lett. B 825 (2022) 136865.

[47] B. Abelev, et al. (STAR), Υ cross section in $p+p$ collisions at $\sqrt{s}$ = 200 GeV, Phys. Rev. D 82 (2010) 012004.

[48] A. Adare, et al. (PHENIX), Measurement of Υ(1S+2S+3S) production in $p+p$ and Au+Au collisions at $\sqrt{s_{NN}}$ = 200 GeV, Phys. Rev. C 91 (2015) 024913.

[49] W. Zha, C. Yang, B. Huang, L. Ruan, S. Yang, Z. Tang,

Z. Xu, Systematic study of the experimental measurements on ratios of different Υ states, Phys. Rev. C 88 (2013) 067901.

[50] L. Y. Zhu, et al. (NuSea), Measurement of Υ Production for $p+p$ and $p+d$ Interactions at 800 GeV/c, Phys. Rev. Lett. 100 (2008) 062301.

[51] D. Acosta, et al. (CDF), Υ Production and Polarization in $p\bar{p}$ Collisions at $\sqrt{s} = 1.8$ TeV, Phys. Rev. Lett. 88 (2002) 161802.

[52] S. Chatrchyan, et al. (CMS), Measurement of the $\Upsilon(1S), \Upsilon(2S)$, and $\Upsilon(3S)$ cross sections in pp collisions at $\sqrt{s} = 7$ TeV, Phys. Lett. B 727 (2013) 101–25.

[53] J.-P. Lansberg, New Observables in Inclusive Production of Quarkonia, Phys. Rept. 889 (2020) 1–106.

[54] N. Brambilla, M. A. Escobedo, M. Strickland, A. Vairo, P. Vander Griend, J. H. Weber, Bottomonium production in heavy-ion collisions using quantum trajectories: Differential observables and momentum anisotropy, Phys. Rev. D 104 (2021) 094049.

[55] N. Brambilla, M. A. Escobedo, M. Strickland, A. Vairo, P. Vander Griend, J. H. Weber, Bottomonium suppression in an open quantum system using the quantum trajectories method, JHEP 05 (2021) 136.

[56] N. Brambilla, M. A. Escobedo, A. Islam, M. Strickland, A. Tiwari, A. Vairo, P. Vander Griend, Heavy quarkonium dynamics at next-to-leading order in the binding energy over temperature, arXiv 2205.10289 (2022).